Energy Advances

Accepted Manuscript

This article can be cited before page numbers have been issued, to do this please use: E. Palmieri, A. Patra, G. Polino, H. J. Lomeri, E. Casagrande, G. Landi, L. La Notte, J. Baker, B. De Jong, F. De Rossi, S. Orlanducci and F. Brunetti, *Energy Adv.*, 2026, DOI: 10.1039/D5YA00352K.

ROYAL SOCIETY OF CHEMISTRY

rsc.li/energy-advances

View Article Online
DOI: 10.1039/D5YA00352K

Fully printed energy storage devices on consumer paper substrates: An eco-friendly approach for low-cost and disposable smart electronics system

Elena Palmieri [1,2,‡], Abhinandan Patra[3,‡], Giuseppina Polino[3], Hamed Javanbakht Lomeri [3], Elisa Casagrande[3], Giovanni Landi[4], Luca La Notte[5], Jenny Baker[6], Bas De Jong [7], Francesca De Rossi [3], Silvia Orlanducci[2], Francesca Brunetti[3,]*

[1] Consiglio Nazionale delle Ricerche, Istituto per la microelettronica e i microsistemi, via del fosso del cavaliere 1, 00133 Rome, Italy

[2] Department of Chemical Science and Technologies, University of Rome Tor Vergata, Via della Ricerca Scientifica 1, 00133 Rome, Italy

[3] CHOSE, Department of Electronic Engineering, University of Rome Tor Vergata, via del Politecnico 1, 00133 Rome, Italy

[4] ENEA - Research Center Portici - P. le Enrico Fermi, 1 Località Granatello -80055 Portici (Napoli)

[5] ENEA - Research Center Casaccia, via anguillarese 301, 00123 Santa Maria di Galeria (Roma)

[6] Faculty of Science and Engineering, Swansea University, Bay Campus, SA1 8EN, UK

[7] Department of Biotechnology, Chemistry and Pharmacy, University of Siena, Via A. Moro 2, Siena 53100, Italy

[8] Faculty of Engineering and Design, University of Bath, Claverton Down, Bath, BA2 7AY

‡ These authors equally contributed to the paper
*Corresponding author

Abstract

The integration of electronic devices into wearable applications has revolutionized the way we interact with technology. The utilization of sustainable materials that align with the principles of environmental consciousness makes it more remarkable. In this context, we propose the fabrication of an energy storage device, supercapacitor, prepared following a ‘‘green approach’’, starting from the substrate used for its fabrication, i.e., various paper-based materials and continuing through to the final step. The device fabrication was achieved through screen printing, a scalable and efficient technique that enables precise deposition of materials while eliminating waste. The electrode component is carbon-based, offering cost-effectiveness and mechanical durability, while the use of sodium alginate as both the electrolyte and the interlayer represents a significant innovation. By serving a dual role, sodium alginate reduces the need for additional materials, simplifying the manufacturing process and lowering the device's overall environmental impact. Sodium alginate, derived from renewable and sustainable sources, possesses exceptional biocompatibility and eco-friendliness. Its high ion conductivity and excellent film-forming capabilities make it particularly

well-suited for flexible and wearable electronic devices. The obtained interdigitated supercapacitor has a power in the range between ~880 μW/Kg and 505 mW/Kg was demonstrated. This approach not only optimizes the device structure but also reduces its ecological footprint, aligning with the growing demand for low-cost green energy technologies and sustainable materials in electronic applications.

1. Introduction

Flexible solid-state supercapacitors (SCs) have attracted great interest due to a growing request of energy in modern portable/wearable electronic devices including mobile phones, laptops, cameras, smartwatches, activity trackers, and health monitoring devices. The increased energy consumption of these smart electronics requires improved energy storage devices with peculiar characteristics: recyclability, biocompatibility, flexibility and low environmental impact both in terms of production and disposal [1]. Batteries based on Li-ion technology, might reach 3000 cycles of charging/discharging but this is not satisfactory for long term applications [2]. In this context, an alternative is represented by supercapacitors which supply moderate energy density, high power rates and long cycle life [3]. Electric double-layer capacitors (EDLCs) are known to exploit the charge accumulation in the electric double-layer. The mechanism is based on the weak electrostatic interaction of ions from the electrolyte bulk with the electrode surface [4]. Unlike batteries, this kind of energy storage device can store the charge physically, and the lack of electrochemical reactions ensures very high power (with a response time up to 1s) and a cyclability of 1,00,000 cycles [3]. When designing a SC, there are many crucial aspects to be taken into consideration, starting from the substrate to be used for the fabrication of the device, to the choice of the electrode and electrolyte and finally, the suitable technique for the fabrication. As for the substrate, commonly used materials include polymers such as polyethylene terephthalate (PET), polyimide (PI), and polyethylene naphthalate (PEN) [5,6] which offer excellent mechanical flexibility and thermal stability, enabling the fabrication of flexible and wearable energy storage devices. They provide a robust template for electrode materials maintaining structural integrity during bending or stretching. Notwithstanding their proven efficacy and pervasive deployment, the necessity for environmentally benign alternatives persists. Significant research efforts [7,8] are now being directed towards the development of energy storage devices utilising paper and paper-like materials. These materials offer a number of significant advantages, including flexibility, lightweight and broad availability, which collectively contribute to a cost-effective and environmentally friendly fabrication process. Despite the fact that paper substrates typically display reduced mechanical strength and thermal stability in comparison to conventional materials, and that their overall processability is more constrained, notable outcomes have been attained [9].

To overcome the lower energy density of SCs, in the last decades, the research on electrodes for SCs began with the investigation of carbon and conducting polymer (CP) based materials [1,10]. Carbon-based materials for supercapacitor electrode fabrication exhibit versatile properties, i.e. a high specific surface area and a well-defined porosity, making them the most popular choice for electrochemical capacitor applications. Moreover, they are suitable for low-cost room temperature techniques such as screen printing [11,12]. It is well known that textural and structural properties of the electrode material play a central role in the final performance of the electrochemical capacitor. Furthermore, it is possible to use activated carbon normally obtained from biomass [13,14]. Likewise, hydrogels, possess promising features for applications in sustainable portable/wearable electronics [15–17] such as stretchability, foldability, and even self-healing ability, and can be employed for the fabrication of both electrodes and electrolytes in devices such as supercapacitors [18–28]. In recent years, it was demonstrated the possibility to realize electrolytes using an environment-friendly and biocompatible polysaccharide, taking the advantage of natural porous structure present in the seaweed, mainly Na- (sodium alginate) and K- derivatives (usually carrageenan ─ a potassium-rich carbohydrate), homogeneously distributed in the bulk of this biomass. The use of porous hydrogel nanostructures provides high flexibility and combines several properties such as easy processability, reduction of the device cost, improved solid–liquid interface, larger electrochemically active surface area, short pathways for charge/mass transport and reliable behaviour during bending cycles [22,24]. For supercapacitors, electrolytes can be categorized into aqueous, organic, and ionic types, each with distinct advantages and limitations [29–31]. Aqueous electrolytes offer high conductivity but have a low dissociation voltage. Organic electrolytes provide higher voltage and broader temperature range but lower conductivity and higher costs. Ionic electrolytes, while stable at higher voltages, exhibit lower conductivity than aqueous or organic electrolytes [31]. Sodium alginate emerges as a sustainable alternative, forming thick, stable gels when combined with metal ions, enabling safe and efficient sodium-ion-based energy storage. Its natural origin, low cost, and excellent film-forming properties make it ideal for environmentally friendly energy applications [23,24,32,33].

In this study, carbon-based interdigitated supercapacitors were fabricated on paper-derived substrates, including copy paper and different consumer papers. These substrates were chosen for their biocompatibility, low cost, and suitability for smart electronics applications. Sodium alginate was employed as a functional interlayer on top of the carbon electrode and as the electrolyte. Comparative analysis of the different paper types revealed that the surface morphology, the texture and the overall structure of the substrate influence the total capacitance of the supercapacitor. We achieved a maximum specific areal capacitance of ~70μF/cm^2 and a gravimetric capacitance of ~280μF/g with copy paper. These findings present exciting prospects for the utilization of diverse paper substrates

View Article Online
DOI: 10.1039/D5YA00352K

in the development of high-performance supercapacitors for energy storage and smart electronics applications.

2. Experimental

2.1 Materials

Carbon-based electrodes were realized using highly conductive thermoplastic carbon paste (Dycotec DM-CAP-4701S). This paste allows fast drying at low temperature (<100˚C) with a sheet resistance of <10 Ω/ /25µm. The electrolyte was realized considering 0.15 gr of Na alginate (Sigma Aldrich) dissolved in 6 ml of deionized water; the functionalization layer that acts as interlayer is prepared using 1.5 gr of Na alginate dissolved in 50 ml of deionized water. Both solutions were stirred for 6 hours at room temperature before use. The Na-alginate solution used as electrolyte showed a slightly lower conductivity, 4.5 mS/cm at 20°C, compared to the interlayer solution (8.7 mS/cm at 20°C), due to the lower polymer amount. Acid-free copy paper with alkaline reserve was provided from Cartiere Miliani Fabriano and disposable paper substrates were supplied from Essity AB industries.

2.2 Device fabrication

The initial stage of the fabrication process for supercapacitors entails the screen printing of the carbon electrodes (Baccini Screen Printers) utilising a printing screen of dimensions 380x460mm with a mesh of 45 µm. The total active area of the electrode was found to be 2.88 cm^2 with the measured fingers having a width of ~1mm and a length of ~15mm. In **Figure 1a** the paper substrates used in the experiments are reported and the fabrication of the interdigitated planar structure based on a carbon-based electrode on the top of different large-area paper substrates is shown in **Figure 1b-c**. After the deposition, the electrodes were sintered in oven at 80°C for 1h and cut to obtain substrates with an area of 4 cm^2. The deposition of electrolyte and interlayer sodium alginate was performed by drop casting methods (**Figure 1d**) and then dried at room temperature overnight in a controlled ambient humidity of 50% RH. More specifically, three different configurations of the supercapacitor were investigated, as reported in the inset of the **Figure 1d**. In the first case, Na-alginate was used in lower concentration (2.4 $\%_w$, 600 µl) as electrolyte directly in contact with the electrode (**Figure 1d-EL**). In the other two cases, an interlayer of Na-alginate (2.9 $\%_w$) was deposited before the deposition of the electrolyte. Two amounts of interlayer were investigated (200 µl, **Figure 1d-I1+EL,** and 400 µl, **Figure 1d-I2+EL**).

View Article Online
DOI: 10.1039/D5YA00352K

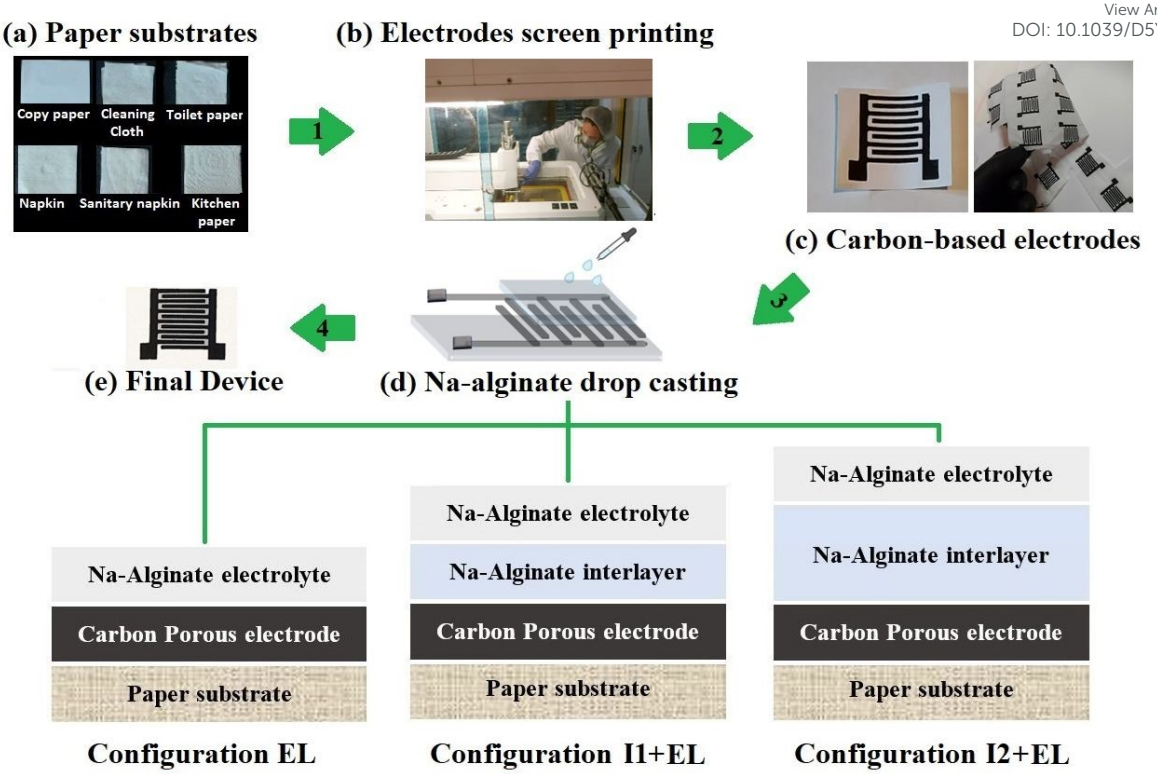

***Figure 1**: Fabrication process of printed supercapacitors: (a) Paper substrates employed in the experiments: copy paper, cleaning cloth, toilet paper, napkin, sanitary napkin, kitchen paper; (b) Screen printing of carbon electrodes; (c) Printed carbon-based electrodes on copy and disposable paper; (d) Deposition of sodium alginate interlayer and/or electrode via drop casting; (e) final device. INSET d: Configuration of the three different supercapacitors investigated. Configuration EL: electrolyte applied directly on the electrode surface; Configuration I1+EL: electrolyte applied on top of Na-Alginate interlayer (200 µl); Configuration I2+EL: electrolyte applied on top of Na-Alginate interlayer (400 µl).*

The deposition of the electrolyte, both for the I1+EL and the I2+EL configurations, was performed after the complete drying of the interlayer. For all three configurations, the devices were characterised as soon after the deposition of the electrolyte (wet) and the day after (dry).

2.3 Rheological characterization of electrolyte and interlayer

Rheological characterization of the Na-alginate-based electrolyte and interlayer was performed using an AR 2000 rheometer (TA Instruments) with a cone and plate measurement geometry, where the cone rotates, imposing a homogeneous strain through the sample, which is placed on the fixed plate. Specifically, a 60 mm diameter 2° acrylic cone was used. The viscosity-shear rate profiles, referred to as 'flow curves', were determined at 25 °C, in a range of shear rates from 0.1 to 1000 s^{-1}.

2.4 Morphological Characterization

Scanning electron microscope (SEM, TESCAN MIRA) was performed to analyse the morphologies of the various paper substrates and of the carbon electrodes interfaced with Na alginate. The thickness was measured using a feeler gauge (Digital Thickness Gauge FD 50, Käfer).

2.5 Materials and Composition analysis

View Article Online
DOI: 10.1039/D5YA00352K

A sample of carbon ink was subjected to Simultaneous Thermal Analysis (STA) analysis. Nitrogen adsorption was carried out using a Micromeritics Tristar Surface analyser with isotherms measured at -196°C, pre-treatment temperature and time was 80°C for the ink and 400°C for the powder for 8 hours. 400 °C was chosen as the pre-treatment temperature for the powder material since STA analysis determined that the binder was removed from the ink at temperatures above 375°C. The BET (Brunauer–Emmett–Teller) surface area calculations were performed on results between partial pressures of 0.08 and 0.25 [34].

2.6 Electrochemical characterization

The electrochemical performances of Cyclic voltammetry (CV), charge-discharge (CH-DIS) and electrochemical impedance spectroscopy (EIS) of the devices were measured on commercial platform (Arkeo - Cicci Research srl) composed by a potentiostat-galvanostat module (up to 1 MHz of bandwidth), a thermal-vacuum stage and a multichannel not-multiplexed module. Specific capacitance (C_s), specific energy (E), and specific power (P) are calculated using the following equations [35,36]:

$$C_{s-CV} = \frac{\int IdV}{v \times m \times \Delta V} \quad \text{Eq. 1}$$

$$C_{s-CH-DIS} = \frac{I \times \Delta T}{m \times \Delta V} \quad \text{Eq. 2}$$

$$E = \frac{1}{2} \times CV^2 \times \frac{1}{3600} \quad \text{Eq. 3}$$

$$P = \frac{E}{\Delta T} \times 3600 \quad \text{Eq. 4}$$

Where I=current, v=scan rate, m= mass loading, V=potential window, T= discharge time.

The aforementioned formulas are expressed in terms of mass loading.

The capacitance by area was calculated according to Eq. 5 and 6.

$$C_{s-CV} = \frac{\int IdV}{v \times A \times \Delta V} \quad \text{Eq. 5}$$

$$C_{s-CH-DIS} = \frac{I \times \Delta T}{A \times \Delta V} \quad \text{Eq. 6}$$

where A= active area of the electrode.

3. Results and Discussion

We studied the rheological behavior of Na-alginate solutions to assess their suitability for common coating and printing techniques. Viscosity is crucial parameter for understanding fluid deformation under shear and its resistance to mechanical stress. Shear rates vary depending on the technique, ranging from 0.1-10 for drop casting to 10-1000000 s^{-1} for high-speed blade coating [37]. In **Figure S1** of the Supporting Information, we reported flow curves for alginate bio-hydrogels, which displayed typical non-Newtonian shear-thinning behavior, common in polymer solutions due to polymer

View Article Online
DOI: 10.1039/D5YA00352K

alignment during shear. We used the Cross model to fit the curves and determine the zero-rate viscosity, finding values of 0.21 Pa·s for the interlayer solution and 0.18 Pa·s for the electrolyte. As expected, the interlayer solution, with a higher polymer concentration, exhibited slightly higher viscosity than the electrolyte solution. Both solutions remained stable within the tested shear rate range, making them suitable for various coating techniques like blade coating, dip-coating, and drop casting, which were used for the fabrication of the device.

To evaluate the performance of carbon-based and alginate-based materials as a function of the substrate's porosity and hygroscopicity, different kinds of disposable cellulose-based wipers and cloths (reported in **Figure 1a**), were taken into consideration. Prior to the fabrication of the supercapacitor, a morphological characterization of the various papers was performed, to determine which were more suitable for the fabrication of a printed device. These papers, despite the fact of being all cellulosic-based materials, differ from one another in terms of robustness, porosity, and fibrous composition. More specifically, the selection of the papers for the fabrication of the devices was based on their compatibility with a uniform screen-printing deposition of the carbon electrodes. Papers presenting both artificial and native fibres were excluded, as the presence of different kinds of fibres could affect the final quality of the deposition due to different affinity (wettability, adsorption, adhesion, etc.) between fibre and carbon pastes [38,39]. The inhomogeneous cohesion between the fibre and the ink is likely to end up in exfoliation, cracking, or other undesirable phenomena which could lead eventually to affect performance of the final device. With regards to the substrate robustness, an excessive thinness and the presence of holes and voids would lead to a strongly uneven deposition of the electrode material, compromising the efficient printing of the electrode pattern and thus, the functionality of the device. From the investigation performed, among the many papers characterised, the choice fell on Cleaning Cloth®, *Tork*® napkins, and *Floralys*® kitchen paper supplied by Essity, and their SEM characterization is reported in **Figure 2**, and each paper was investigated at different magnification, from the lower (left column) to the higher magnification (right column). Common copy paper was used as reference substrate due to its robustness and high compatibility with printing techniques[28] and its SEM characterization is also reported in **Figure 2a**.

View Article Online
DOI: 10.1039/D5YA00352K

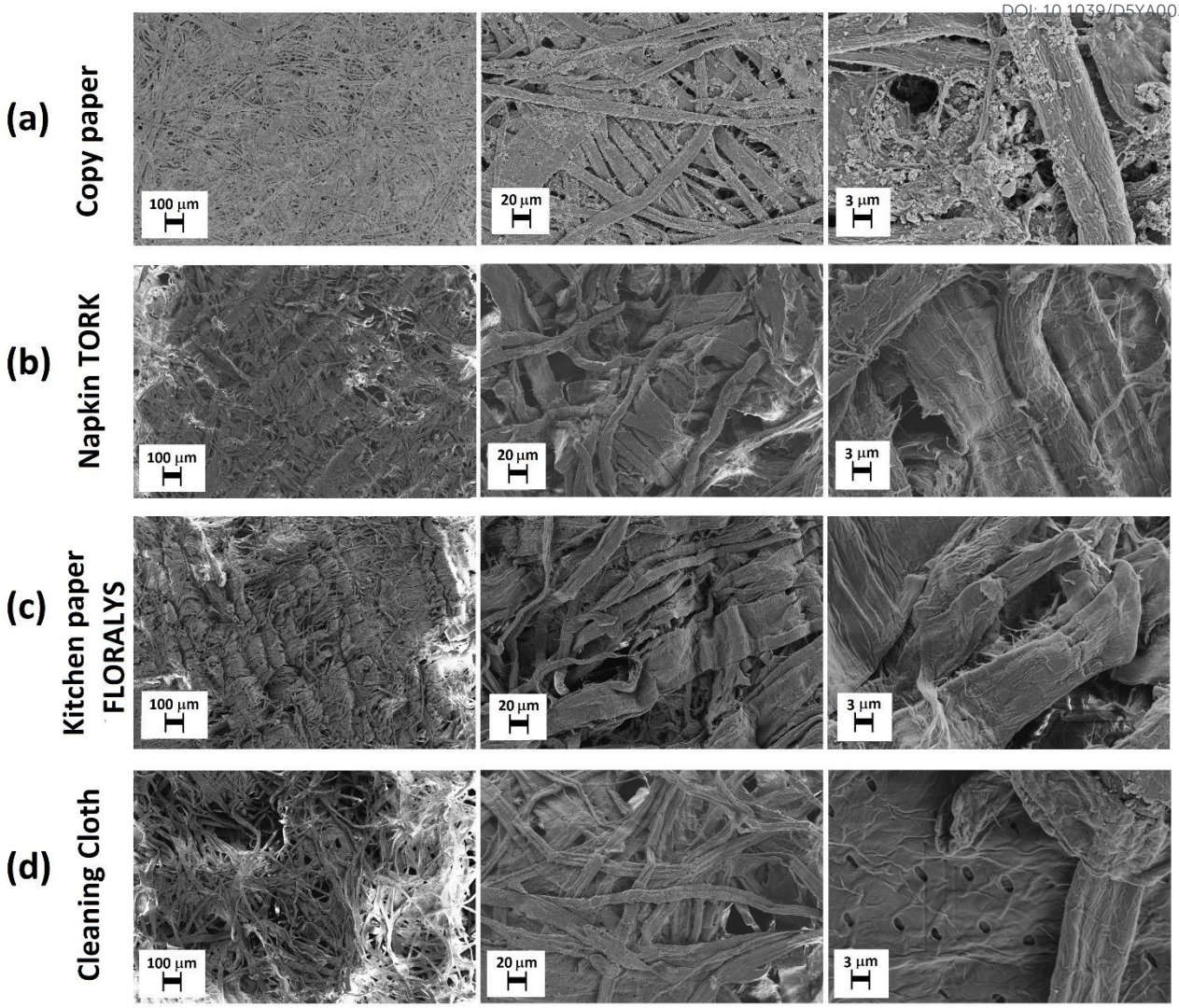

Figure 2: SEM characterization of (a) Copy paper; (b) Napkin TORK; (c) Kitchen paper FLORALYS; (d) Cleaning Cloth.

Figure 2a illustrates the typical fibrous structure of copy paper, observed in three different magnifications. The fibres have an average width of 15 µm. In the case of Napkin *Tork* ® (**Figure 2b**), it is possible to notice a rather compact structure. From SEM image at lower magnification a knitted arrangement in the distribution of the fibres is observable. Fibres show an average width of around 15 µm. With regards to *Floralys*® kitchen paper (**Figure 2c**), a relatively compact structure can be observed. From SEM image at lower magnification a curled/wave-like arrangement is observable. Fibres show an average width of around 15 µm. As for the Cleaning Cloth® (**Error! Reference source not found.2d**), from the SEM image at lower magnification a rather disordered fibrous structure is observable, characterized by only native cellulose fibres, with an average width of around 15-20 µm. At higher magnification it is possible to observe a dotted pattern, which could be due to industrial processing. Hence, based on the SEM analysis, Cleaning Cloth® paper has been

View Article Online
DOI: 10.1039/D5EA00252K

discarded for the following experiments because of its disorganized structure. The morphology of bare carbon-based electrodes, and carbon electrode coated with electrolyte and with interlayer and electrolyte, were investigated. In **Figure 3a** we report the morphology of electrodes deposited on different paper substrates, revealing a compact structure of all the carbon electrodes regardless of the type of cellulose matrix. As reported in SI (**Figure S2**), in all cases, the carbon electrode shows a granular morphology. The presence of the electrolyte (**Figure 3b**) increases the homogeneity of the surface of the device, even though some surface defects such as bubbles and delamination areas can be observed. The use of an interlayer on the top of the carbon electrode (**Figure 3c**) leads to an even more uniform morphology. In this case, some bubbles were also observed, likely caused by air trapped during the coating process. The interlayer interface on the carbon electrode enables a significantly improved and more uniform deposition of the electrolyte. No notable morphological differences were observed among the various types of paper, as the interlayer + electrolyte system effectively envelop and cover the paper's fibrous structure.

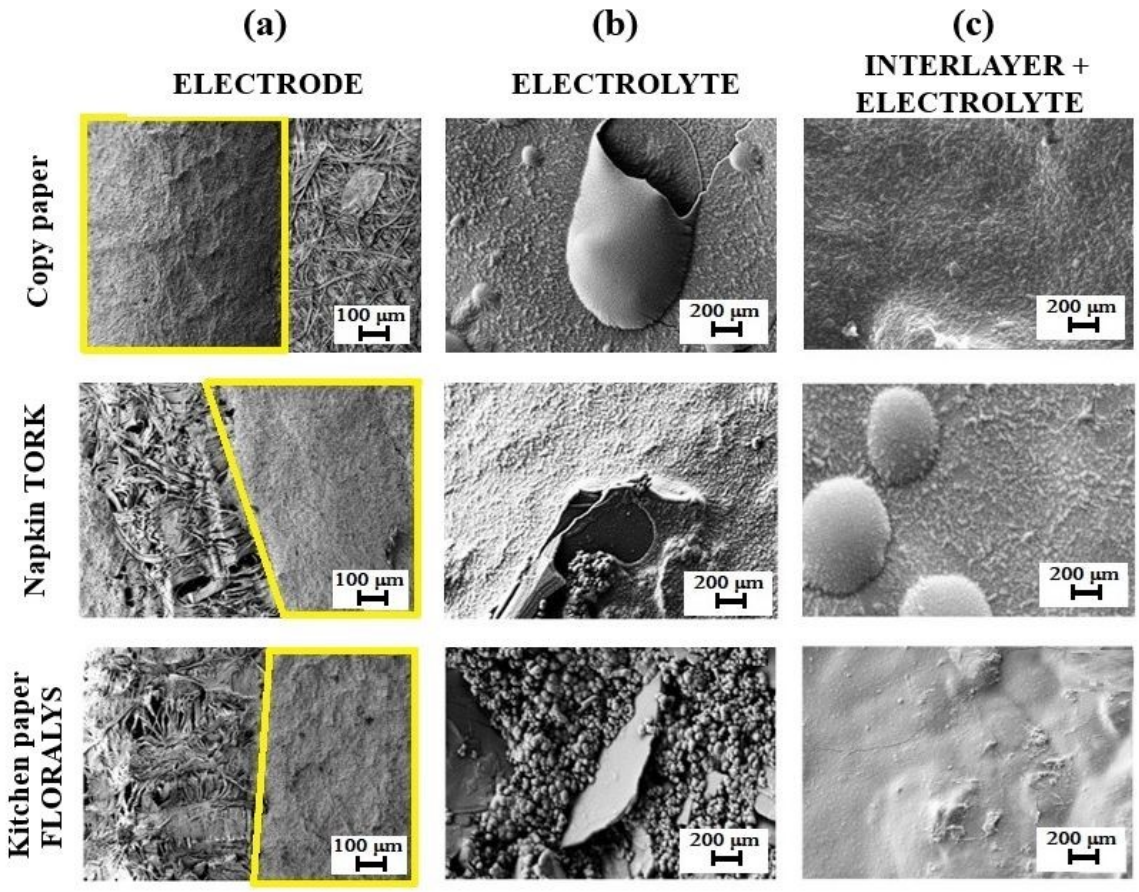

***Figure 3**: SEM micrograph of (a) carbon electrode (yellow box), (b) carbon electrode + Na alginate electrolyte, (c) carbon electrode + Na alginate interlayer + Na alginate electrolyte deposited on Copy paper, Napkin paper TORK, Kitchen paper FLORALYS.*

Additionally, we performed a surface area analysis on both the carbon ink and the carbon active material (eg the powder remaining after thermal removal of the polymeric binder). Whilst it is not the

View Article Online
DOI: 10.1039/D5EY00352K

purpose of this work to optimises the carbon electrode it is important to measure the surface area to allow comparison with other literature. Most research focuses on the surface area of the active material but this is only part of the understanding [40]. For this material the isotherms show limited hysteresis (**Figure 4**) and indicate slit like pores typical of graphitic materials. The surface area of the electrode (including binder) was 2.7 m^2/g whereas the surface area of the active carbon material was 23.2m^2/g denoting a 10-fold reduction in surface area after the introduction of the binder (**Figure 4**). This is typical behaviour of inks where the binder can significantly reduce the apparent surface area of a coating and is a compromise between ink printability / electrode robustness and the available active surface area [41,42].

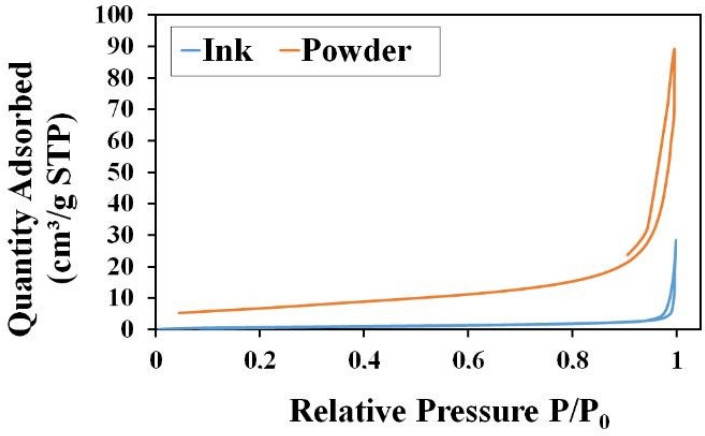

***Figure 4**: Isotherms of the carbon ink and the ink active materials (powder) once the binder contained in the ink has been removed.*

Consequently, the full potential of the active material in terms of surface area cannot be fully realized. Despite the surface area of the electrode being orders of magnitude lower than the active material the devices exhibit noteworthy performance owing to the high paper surface area, especially when compared with substrates like glass, silicon, PET, PI, PEN, and others [32,43].

Supercapacitors were fabricated on all four substrates: Copy paper, Napkin TORK, Kitchen paper FLORALYS and Cleaning Cloth; however, the thin and delicate nature of Napkin TORK made it prone to damage during the screen-printing process, presenting significant challenges in device fabrication. The three configurations (EL, I1+EL, and I2+EL) were first examined on copy paper used as reference substrate. The performance of the devices was tested for all three configurations both before and after the electrolyte drying process, referred to as Wet and Dry devices, respectively. In the case of Dry-device measurements, the electrolyte was allowed to dry overnight at room temperature before testing. In **Table S1** the thicknesses of the device at the various configurations are reported.

The CV profiles of devices on copy paper were recorded in a range from 10 to 100 mV/s (**Figure 5a-c**), for all the configurations, both Wet and Dry. **Figure 5d** displays the comparative CV graphs at 80 mV/s for all the configurations. The CV indicated the capacitive behavior of the devices, showcasing excellent rate capability and reversibility across all the investigated scan rates. A growing capacitive behavior is evident with the presence of the interlayer, observed in both the Wet and Dry devices. As expected, superior performances were attained with the Wet devices, due to major ionic mobility and availability at the electrode surface. Nevertheless, acceptable capacitive behavior was still achieved with the Dry devices, particularly in the case of configuration with the interlayer (**Figure 5b,c**). It should be noted that subtle alterations in the CV curves are noticeable at extremely low scan rates with small oxidation and reduction peaks which could be ascribed to the surface faradic reactions taking place in the electrode and electrolyte interface. This phenomenon can be owing to the electrolytic ions Na^+ [44,45] intercalation/deintercalation during the charge/discharge cycles. At higher scan rates, the capacitive contribution becomes predominant [46], and these alterations are no longer present. The capacitance values for all three configurations for both Wet and Dry devices are reported in **Table 1.** From the collected data one can conclude that the presence of the interlayer improves the performance of the device. However, no significant improvement was observed increasing the thickness of the interlayer. In fact, similar values were found for the configurations I1+EL and I2+EL. Additionally, the presence of the interlayer has a more pronounced impact on the performance of the Dry device compared to the Wet devices. The power law has been employed to analyse the faradic redox reaction, which influences the diffusion-controlled process, as well as the surface-bound supercapacitive kinetics that determine the capacitive response. These contributions have been quantified using the equations provided below.[47,48]

$$i = av^b \qquad \text{Eq.7}$$

$$log\ i = b\ log\ v + log\ a \qquad \text{Eq.8}$$

All parameters used here retain their standard meanings: i represents current, ν denotes the scan rate, and a and b are variables. The value of b indicates the dominant contribution, b = 0.5 signifies a diffusion-controlled process, while b = 1 suggests a capacitive contribution. The value of 'b' between 0.5 and 1 implies a mixed contribution from both mechanisms.

$$i(V) = k_1 + k_2 v^{1/2} \qquad \text{Eq. 9}$$

$$i(V)/\ v^{1/2} = k_1 v^{1/2} + k_2 \qquad \text{Eq. 10}$$

The quantitative assessment of the contribution was carried out using the above equation in conjunction with Dunn's method. In this analysis, k1 and k2 correspond to the slope and intercept

values derived from the linear fitting. At a scan rate of 40 mV/s, the capacitive contribution was observed to be 84.5%, while the diffusion-controlled component accounted for 14.5% (**Fig. S3a**). Likewise, as the scan rate decreased from 40 to 20 mV/s, the capacitive contribution gradually declined from 84.5% to 80%, similarly when the scan rates increased the capacitive contribution also increased, confirming the predominantly capacitive nature of the electrode over battery-type behaviour (**Fig. S3b**).

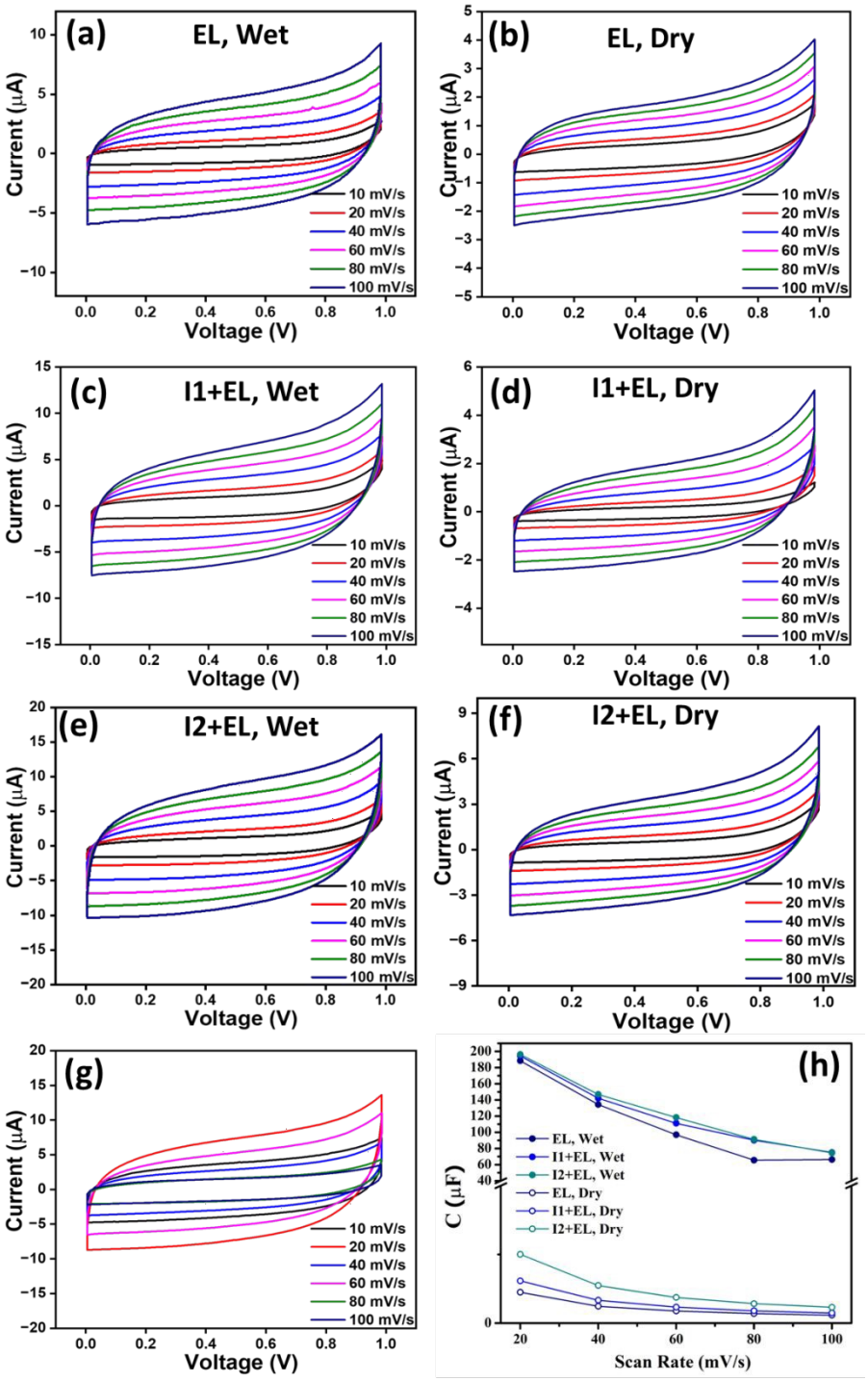

***Figure 5**: CV characterization for copy paper-based devices, with the three configurations tested (a,b) at various scan rates for the configuration EL (only electrolyte), Wet and Dry devices; (c,d) at various scan rates for the I1+EL (interlayer 200µl+ electrolyte), Wet and Dry devices; (e,f) at various scan rates for the I2+EL (interlayer 400µl+ electrolyte), Wet and Dry devices; (g) at a fixed scan*

View Article Online
DOI: 10.1039/D5YA00352K

rate of 80 mV/s, for the Wet and Dry devices; (h) Capacitance as a function of the scan rate for the various configurations tested.

The charge-discharge plots for copy paper in the Wet configuration are reported in **Figure 6a-c**, and further characterization is reported in **Figure S4** of SI. From these measures we extracted the power performance of each architecture: faster charge-discharge in the case of interlayer-based devices in Dry device has been observed, leading to a dramatic increase in Power (**Table 1**) with respect to wet devices. The stability up to 5000 charge-discharge [49] cycles was investigated for all three configurations, both Wet and Dry, and graphs are reported in **Figure 6d.** It is evident that in Wet devices, the capacitance decreases as the electrolyte dries out. Once the electrolyte is fully dried, the capacitance values stabilize, although at significantly lower levels (up to -80% after 5000 cycles). The behavior is more stable for configurations with the interlayer, which exhibit a more gradual decrease in capacitance over time. Similarly, in Dry devices, the configurations with the interlayer demonstrate a more stable response, showing around a 40% increase in capacitance. In the configuration without the interlayer, around an 80% loss in capacitance is observed after 5000 cycles with more than 96% of columbic efficiency.

Figure S5 presents the results of the EIS investigation for the three configurations. The figure highlights a shift in the equivalent series resistance (ESR), estimated from the x-intercept of the EIS spectra, towards lower resistance values with the incorporation of I1 and I2. This reduction in ESR enhances the supercapacitor's energy storage and delivery capabilities, thereby improving its overall energy performance. In the case of copy paper, the data demonstrate that the presence of the interlayer significantly enhances capacitance behaviour. The improved electrochemical performance observed in the copy paper with the I2+EL configuration can be attributed to the lower solution resistance (R_s) and charge transfer resistance (R_{ct}) of the electrode compared to other configurations. This improvement is likely due to the increased active surface area facilitated by this specific configuration [19,50,51]. This finding aligns with previous literature on the role of sodium alginate in relation to carbon electrodes[1,32].After examining the role of the interlayer in the context of the reference copy paper, we proceeded to evaluate the device performance using the other types of paper. Given that no significant difference was observed among the configurations with the different thicknesses of the interlayer, the I1+EL configuration is the preferred choice in terms of both device performance and cost-effectiveness. Consequently, the EL and I1+EL configurations were studied for the other two types of paper substrates.

View Article Online
DOI: 10.1039/D5YA00352K

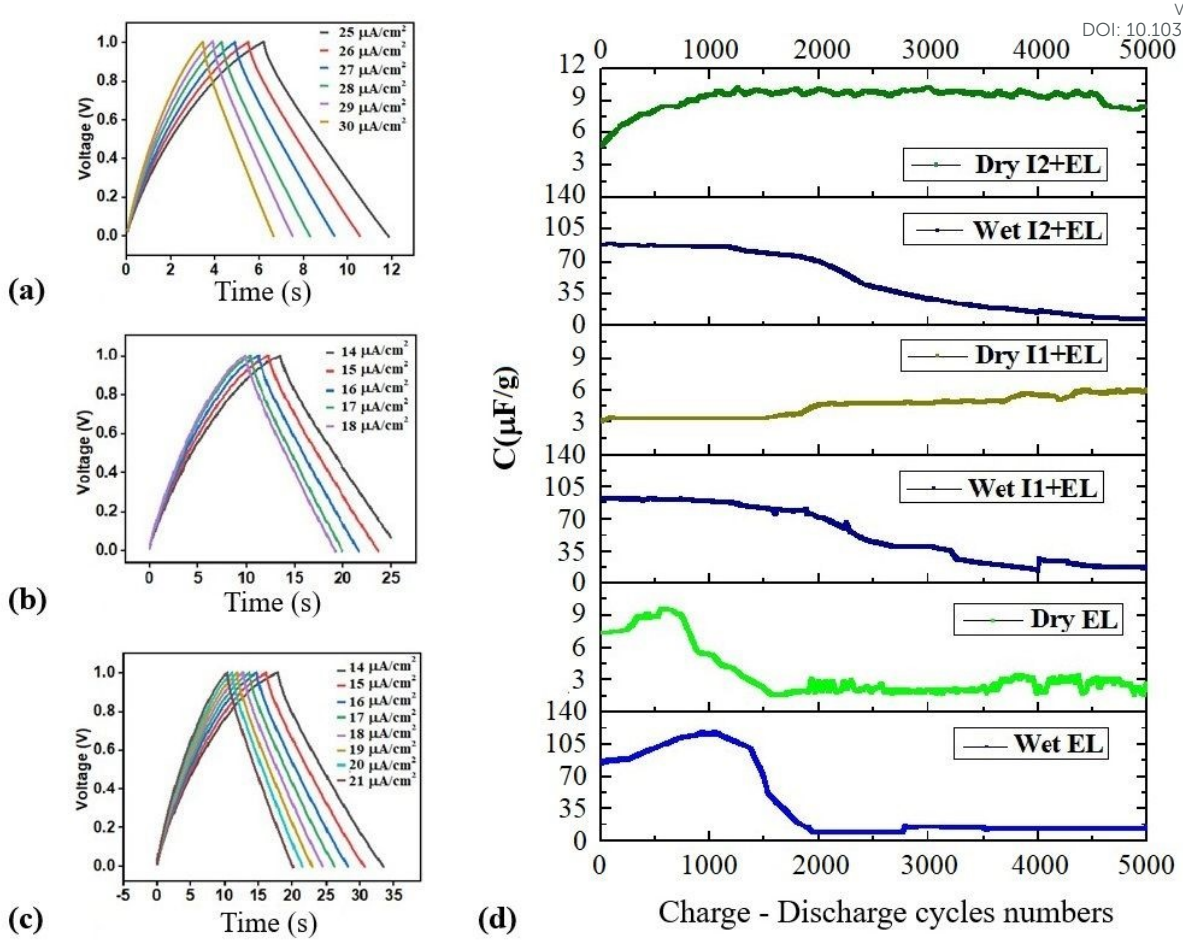

Figure 6: *Charge-Discharge for reference devices on copy paper (a) Wet EL configuration (b) Wet I1+EL (c) Wet I2+EL, (d) Cyclic stability up to 5000 cycles for the EL configuration, Wet and Dry, I1+EL configuration, Wet and Dry, I2+EL configuration, Wet and Dry.*

Table 1*: Performance achieved for various paper substrates, with different device configurations. n.a.= not applicable, in case of non-functioning device or configuration.*

		C	C_{sp}	C_{sp}	P_{area}	P_{mass}	E_{area}	E_{mass}	Q
		(µF)	*(µF/cm²)*	*(µF/g)*	*(µW/cm²)*	*(µW/g)*	*(µWh/cm²)*	*(µWh/kg)*	*(µAh)*
Copy paper	EL, Wet	188.4	65.4	306.4	21.8	102.0	36.3×10^{-3}	170.2	0.105
	I1+EL, Wet	194.4	67.5	236.8	13.5	47.4	36.9×10^{-3}	131.6	0.108
	I2+EL, Wet	196.3	68.2	191.1	13.6	38.2	36.5×10^{-3}	106.2	0.109
	EL, Dry	5.3	1.9	354.7	1.1	202.7	1.02×10^{-3}	197.0	0.0030
	I1+EL, Dry	7.78	2.7	370.5	4.2	570.0	1.50×10^{-3}	205.8	0.0043
	I2+EL, Dry	10.0	3.5	370.7	4.1	436.2	1.93×10^{-3}	206.0	0.0056

View Article Online
DOI: 10.1039/D5YA00352K

Kitchen paper	EL, Wet	290.5	100.8	472.3	16.1	75.6	56.0 x10^{-3}	262.4	0.161
	I1+EL, Wet	319.3	110.9	310.9	44.3	124.4	61.6 x10^{-3}	172.7	0.177
	EL, Dry	0.71	0.2	47.1	n.a.	n.a.	0.1 x10^{-3}	26.1	0.00040
	I1+EL, Dry	8.26	2.9	305.9	4.6	489.5	1.6 x10^{-3}	170.0	0.0046
Napkin paper	EL, Wet	287.5	99.8	467.5	79.9	374.0	55.5 x10^{-3}	259.7	0.160
	I1+EL, Wet	180.9	62.8	176.1	251.3	704.6	34.9 x10^{-3}	97.8	0.100
	EL, Dry	n.a.	n.a.	n.a.	n.a.	n.a.	n.a.	n.a.	n.a.
	I1+EL, Dry	3.47	1.2	128.5	n.a.	n.a.	0.7 x10^{-3}	71.4	0.00193

In **Figure S6**, we present the comparison of the CV curves within the potential window (-1 to 1V for Dry devices, -0.75 to 0.75 V for Wet devices) at a scan rate of 100 mV/s for both kitchen and napkin papers, with the data summarized in **Table 1**. This experiment was performed to observe the electrochemical response of the devices during both the negative and positive scans, ensuring a complete assessment of their charge–discharge behaviour and verifying the symmetry of the CV profiles across the potential window. As evident from the data, the porosity and absorbent properties of the paper significantly influence the capacitive behaviour. Both devices on kitchen paper and napkin paper exhibit slightly higher capacities than that of copy paper.

For kitchen paper, the interlayer improves device performance, especially in the Dry configuration. Conversely, for napkin paper, the presence of the interlayer reduces device performance in the Wet configuration. This effect is attributed to the delicate nature of paper; the interlayer and electrolyte depositions during device fabrication exert excessive stress on the paper, causing it to swell during deposition and shrink while drying, leading to deformation of the paper substrate, ultimately affecting device functionality. However, once again the interlayer has a noteworthy positive effect on the Dry device. In fact, while a functioning Dry device could not be achieved with the EL configuration, decent performance was obtained with the I1+EL configuration.

In **Figure S7**, we present a comparison of the charge-discharge plots for devices prepared on commercial paper substrates. It was not possible to obtain charge-discharge cycles for supercapacitors in the EL Dry configuration for either Kitchen or Napkin paper. However, for the Dry configuration, we successfully achieved charge-discharge cycles for the I1+EL configuration using Kitchen Paper. For these types of paper, the configuration incorporating the interlayer demonstrated faster cycles compared to the configuration without it, which contrasts with the behaviour observed on copy paper. This is probably due to the intrinsic morphological differences between these paper samples. Figure

S8 shows the CV and GCD curves of the devices connected in series and parallel configuration signifying the reproducibility of the devices and its application in real time.

The performances of our devices are reported in the Ragone plot (**Figure 7**) as well as in Table S2 in the supplementary file , comparing them with the recent study proposed by Zhao et al. that used the same electrolyte on plastic polyimide, achieving a power density of 0.18 mW/cm² and an energy density of 21.20 µWh/cm² [23]. Building on this work, we are the first to successfully develop supercapacitors on commercial and disposable paper substrates using Na-alginate eco-friendly hydrogel demonstrating the critical importance of the combination of substrate porosity and device architecture in influencing the overall performance of the device.

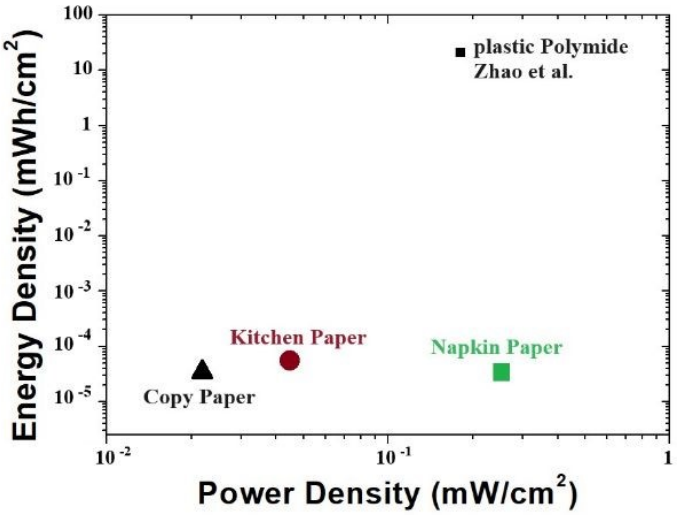

***Figure 7**: Ragone plot of the printed supercapacitors on paper and reference device on plastic from literature.*

4. Conclusion

In this preliminary investigation, we have successfully demonstrated the feasibility of fabricating energy storage devices on disposable and biodegradable paper substrates commonly used in everyday life. We used Na-alginate eco-friendly hydrogel as an electrolyte, and we were able to tune the architecture and performance of the devices by using Na-alginate at a different concentration as an interlayer between the carbon-based electrodes and the electrolytic layer. Furthermore, we confirmed the compatibility of cellulose-based substrate materials with the fabrication of electrical devices using large-area printing methods and biocompatible, biodegradable raw materials. This work lays the groundwork for developing smart supercapacitors on unconventional and flexible substrates. We achieved a power density of 251 µW/cm² and an energy density of 62 nWh/cm² on paper substrates, without resorting to harsh chemicals or unsustainable materials, underscoring the potential for the much-needed high-performing, environmentally friendly energy storage solutions.

View Article Online
DOI: 10.1039/D5YA00352K

Acknowledgements

The authors acknowledge the European H2020 project, "Wearable Applications enabled by electronic Systems on Paper (WASP)" (no. 825213). We acknowledge funding from the UKRI – EPSRC through TReFCo EP/W019167/1 (JB).

The supporting data has been provided as part of the Supplementary information. Supplementary information: Figure S1-S8 SEM images, electrochemical performance and Table S1 for the comparative table comparing the figure of merit with the state of the art.

References

1. Pérez-Madrigal, M. M., Estrany, F., Armelin, E., Díaz, D. D. & Alemán, C. Towards sustainable solid-state supercapacitors: electroactive conducting polymers combined with biohydrogels. *J. Mater. Chem. A* **4**, 1792–1805 (2016).
2. Jiang, Y. & Song, W. Predicting the Cycle Life of Lithium-Ion Batteries Using Data-Driven Machine Learning Based on Discharge Voltage Curves. *Batteries* **9**, 413 (2023).
3. Gul, H., Shah, A.-H. A. & Bilal, S. Achieving Ultrahigh Cycling Stability and Extended Potential Window for Supercapacitors through Asymmetric Combination of Conductive Polymer Nanocomposite and Activated Carbon. *Polymers* **11**, 1678 (2019).
4. Patra, A. *et al.* Understanding the charge storage mechanism of supercapacitors: in situ/operando spectroscopic approaches and theoretical investigations. *J. Mater. Chem. A* **9**, 25852–25891 (2021).
5. Latest advances in substrates for flexible electronics - MacDonald - 2007 - Journal of the Society for Information Display - Wiley Online Library. https://sid.onlinelibrary.wiley.com/doi/abs/10.1889/1.2825093.

6. Hassan, M. *et al.* Significance of Flexible Substrates for Wearable and Implantable Devices: Recent Advances and Perspectives. *Adv. Mater. Technol.* **7**, 2100773 (2022).
7. Beg, M. *et al.* Paper Supercapacitor Developed Using a Manganese Dioxide/Carbon Black Composite and a Water Hyacinth Cellulose Nanofiber-Based Bilayer Separator. *ACS Appl. Mater. Interfaces* **15**, 51100–51109 (2023).
8. Dissanayake, K. & Kularatna-Abeywardana, D. A review of supercapacitors: Materials, technology, challenges, and renewable energy applications. *J. Energy Storage* **96**, 112563 (2024).
9. Thakur, A. & Devi, P. Paper-based flexible devices for energy harvesting, conversion and storage applications: A review. *Nano Energy* **94**, 106927 (2022).
10. Raymundo-Piñero, E., Leroux, F. & Béguin, F. A High-Performance Carbon for Supercapacitors Obtained by Carbonization of a Seaweed Biopolymer. *Adv. Mater.* **18**, 1877–1882 (2006).
11. Cancelliere, R. *et al.* Expanding the circularity of plastic and biochar materials by developing alternative low environmental footprint sensors. *Green Chem.* **25**, 6774–6783 (2023).
12. Palmieri, E., Cancelliere, R., Maita, F., Micheli, L. & Maiolo, L. An ethyl cellulose novel biodegradable flexible substrate material for sustainable screen-printing. *RSC Adv.* **14**, 18103–18108 (2024).
13. Herou, S., Schlee, P., Jorge, A. B. & Titirici, M. Biomass-derived electrodes for flexible supercapacitors. *Curr. Opin. Green Sustain. Chem.* **9**, 18–24 (2018).
14. Zhai, Z., Ren, B., Xu, Y. & Liu, Z. Metal-doped carbon aerogel from sodium alginate for supercapacitor. *IOP Conf. Ser. Mater. Sci. Eng.* **592**, 012077 (2019).
15. Cui, C. *et al.* Recent Progress in Natural Biopolymers Conductive Hydrogels for Flexible Wearable Sensors and Energy Devices: Materials, Structures, and Performance. *ACS Appl. Bio Mater.* **4**, 85–121 (2021).
16. Palmieri, E. *et al.* A Sustainable Hydroxypropyl Cellulose-Nanodiamond Composite for Flexible Electronic Applications. *Gels* **8**, 783 (2022).

17. Maita, F. *et al.* Application of Unconditioned Nanostructured Thermoplastic-Based Strain Gauge Sensor in Wearable Electronics. *IEEE Sens. J.* **PP**, 1–1 (2022).
18. Landi, G., Granata, V., Germano, R., Pagano, S. & Barone, C. Low-Power and Eco-Friendly Temperature Sensor Based on Gelatin Nanocomposite. *Nanomaterials* **12**, 2227 (2022).
19. Landi, G. *et al.* Regeneration and Long-Term Stability of a Low-Power Eco-Friendly Temperature Sensor Based on a Hydrogel Nanocomposite. *Nanomaterials* **14**, 283 (2024).
20. Landi, G. *et al.* Impact of Acetate-Based Hydrogel Electrolyte on Electrical Performance and Stability of Eco-Friendly Supercapacitors. *ChemElectroChem* **10**, (2023).
21. Landi, G., La Notte, L., Palma, A. L. & Puglisi, G. Electrochemical Performance of Biopolymer-Based Hydrogel Electrolyte for Supercapacitors with Eco-Friendly Binders. *Polymers* **14**, 4445 (2022).
22. Menzel, J., Frąckowiak, E. & Fic, K. Agar-based aqueous electrolytes for electrochemical capacitors with reduced self-discharge. *Electrochimica Acta* **332**, 135435 (2020).
23. Zhao, J. *et al.* Preparation of the polyelectrolyte complex hydrogel of biopolymers via a semi-dissolution acidification sol-gel transition method and its application in solid-state supercapacitors. *J. Power Sources* **378**, 603–609 (2018).
24. Zhao, W., Wei, L., Fu, Q. & Guo, X. High-performance, flexible, solid-state micro-supercapacitors based on printed asymmetric interdigital electrodes and bio-hydrogel for on-chip electronics. *J. Power Sources* **422**, 73–83 (2019).
25. Wang, K. *et al.* Electrodeposition of alginate with PEDOT/PSS coated MWCNTs to make an interpenetrating conducting hydrogel for neural interface. *Compos. Interfaces* **26**, 27–40 (2019).
26. Babeli, I. *et al.* Conductive, self-healable and reusable poly(3,4-ethylenedioxythiophene)-based hydrogels for highly sensitive pressure arrays. *J. Mater. Chem. C* **8**, 8654–8667 (2020).
27. Han, Y. & Dai, L. Conducting Polymers for Flexible Supercapacitors. *Macromol. Chem. Phys.* **220**, 1800355 (2019).

28. Polino, G. *et al.* Nanodiamond-Based Separators for Supercapacitors Realized on Paper Substrates. *Energy Technol.* **8**, 1901233 (2020).

29. Collins, J., Gourdin, G. & Qu, D. Modern Applications of Green Chemistry. in *Green Chemistry* 771–860 (2018). doi:10.1016/B978-0-12-809270-5.00028-5.

30. Xia, L., Yu, L., Hu, D. & Chen, G. Z. Electrolytes for electrochemical energy storage. *Mater. Chem. Front.* **1**, 584–618 (2017).

31. Yu, L. & Chen, G. Z. Ionic Liquid-Based Electrolytes for Supercapacitor and Supercapattery. *Front. Chem.* **7**, (2019).

32. Zeng, J., Wei, L. & Guo, X. Bio-inspired high-performance solid-state supercapacitors with the electrolyte, separator, binder and electrodes entirely from: Kelp. *J. Mater. Chem. A* **5**, 25282–25292 (2017).

33. Zhang, R., Wang, L., Zhao, J. & Guo, S. Effects of Sodium Alginate on the Composition, Morphology, and Electrochemical Properties of Electrospun Carbon Nanofibers as Electrodes for Supercapacitors. *ACS Sustain. Chem. Eng.* **7**, 632–640 (2019).

34. Brunauer, S., Emmett, P. H. & Teller, E. Adsorption of Gases in Multimolecular Layers. *J. Am. Chem. Soc.* **60**, 309–319 (1938).

35. Gupta, G., Diwedi, A., Sharma, A. & Shandilya, K. *Hierarchical NiMn Double Layered/Graphene with Excellent Energy Density for Highly Capacitive Supercapacitors*. (2021). doi:10.21203/rs.3.rs-1188443/v1.

36. Taer, E. *et al.* The relationship of surface area to cell capacitance for monolith carbon electrode from biomass materials for supercapacitor aplication. *J. Phys. Conf. Ser.* **1116**, 032040 (2018).

37. Zhu, S. *et al.* Insights into the rheological behaviors evolution of alginate dialdehyde crosslinked collagen solutions evaluated by numerical models. *Mater. Sci. Eng. C* **78**, 727–737 (2017).

38. Plazonić, I., Bates, I. & Barbaric-Mikocevic, Z. The Effect of Straw Fibers in Printing Papers on Dot Reproduction Attributes, as Realized by UV Inkjet Technology. *BioResources* **11**, 5033–5049 (2016).

39. Paszkowska, K., Podsiadlo, H. & Ambroziewicz, A. Influence of the fibre composition of paper containing synthetic fibres on printing properties. *Pap. Technol.* **46**, 21–29 (2005).

40. Pandolfo, A. G. & Hollenkamp, A. F. Carbon properties and their role in supercapacitors. *J. Power Sources* **157**, 11–27 (2006).

41. Baker, J. A. *et al.* Development of Graphene Nano-Platelet Ink for High Voltage Flexible Dye Sensitized Solar Cells with Cobalt Complex Electrolytes. *Adv. Eng. Mater.* **19**, 1600652 (2017).

42. Matshitse, R. & Nyokong, T. Substituent effect on the photophysical and nonlinear optical characteristics of Si phthalocyanine – Detonated nanodiamond conjugated systems in solution. *Inorganica Chim. Acta* **504**, 119447 (2020).

43. Bai, Q., Xiong, Q., Li, C., Shen, Y. & Uyama, H. Hierarchical porous carbons from a sodium alginate/bacterial cellulose composite for high-performance supercapacitor electrodes. *Appl. Surf. Sci.* **455**, 795–807 (2018).

44. Lomeri, H. J. *et al.* Integration of a Paper-Based Supercapacitor and Flexible Perovskite Mini-Module: Toward Self-Powered Portable and Wearable Electronics. *Adv. Funct. Mater.* **34**, 2313267 (2024).

45. Ahmadpour, S., Tashkhourian, J. & Hemmateenejad, B. The effect of carbonaceous materials on faradaic and charging current contribution in carbon paste electrodes investigated by chemometrics methods. *J. Solid State Electrochem.* **23**, 3255–3266 (2019).

46. Pholauyphon, W., Charoen-amornkitt, P., Suzuki, T. & Tsushima, S. Perspectives on accurately analyzing cyclic voltammograms for surface- and diffusion-controlled contributions. *Electrochem. Commun.* **159**, 107654 (2024).

47. Patra, A., Shaikh, M., Ghosh, S., Late, D. J. & Rout, C. S. MoWS2 nanosheets incorporated nanocarbons for high-energy-density pseudocapacitive negatrode material and hydrogen evolution reaction. *Sustain. Energy Fuels* **6**, 2941–2954 (2022).

48. Patra, A. *et al.* All-solid-state flexible supercapacitor based on a binary transition metal dichalcogenide grown on 2D/2D heterostructure materials. *J. Energy Storage* **68**, 107825 (2023).

49. Zhang, J., Gu, M. & Chen, X. Supercapacitors for renewable energy applications: A review. *Micro Nano Eng.* **21**, 100229 (2023).

50. Deng, J., Li, J., Song, S., Zhou, Y. & Li, L. Electrolyte-dependent supercapacitor performance on nitrogen-doped porous bio-carbon from gelatin. *Nanomaterials* **10**, (2020).

51. Landers, J., Gor, G. Y. & Neimark, A. V. Density functional theory methods for characterization of porous materials. *Colloids Surf. Physicochem. Eng. Asp.* **437**, 3–32 (2013).

TOR VERGATA
UNIVERSITÀ DEGLI STUDI DI ROMA

Macroarea di Ingegneria
Dipartimento di Ingegneria Elettronica

View Article Online
DOI: 10.1039/D5YA00352K

To: The Editor, RSC Energy Advances

Dear Editor-in-Chief,

Data for this article, including the electrical characterization and the SEM images are available at https://zenodo.org/ at 10.5281/zenodo.15482834.

Sincerely,
Francesca Brunetti*
(on behalf of all authors)

***Corresponding Author**
Francesca Brunetti
Department of Industrial Engineering, University of Rome Tor Vergata
Email: francesca.brunetti@uniroma2.it